Following the Nonthermal Phase Transition in Niobium Dioxide by Time-Resolved Harmonic Spectroscopy

Nie, Z.; Guery, L.; Molinero, E.B.; Juergens, P.; Van Den Hooven, T.J.; Wang, Y.; Jimenez Galan, A.; Planken, P.C.M.; Silva, R.E.F.; Kraus, P.M.

DOI
10.1103/PhysRevLett.131.243201

Publication date
2023

Document Version
Final published version

Published in
Physical Review Letters

Following the Nonthermal Phase Transition in Niobium Dioxide by Time-Resolved Harmonic Spectroscopy

Z. Nie,[1,*] L. Guery,[1] E. B. Molinero,[2] P. Juergens,[1,3] T. J. van den Hooven,[1] Y. Wang,[4] A. Jimenez Galan,[3] P. C. M. Planken,[1,5] R. E. F. Silva,[2,3] and P. M. Kraus[1,6,†]

[1]*Advanced Research Center for Nanolithography, Science Park 106, 1098 XG Amsterdam, The Netherlands*
[2]*Instituto de Ciencia de Materiales de Madrid, Consejo Superior de Investigaciones Científicas (ICMM-CSIC), E-28049 Madrid, Spain*
[3]*Max-Born-Institute for Nonlinear Optics and Short Pulse Spectroscopy, Max-Born-Strasse 2A, D-12489 Berlin, Germany*
[4]*School of Physics and Electronic Engineering, Taishan University 525 Dongyue Street, Tai'an, Shandong, China*
[5]*Van der Waals-Zeeman Institute, University of Amsterdam, Science Park 904, 1098 XH Amsterdam, The Netherlands*
[6]*Department of Physics and Astronomy, and LaserLaB, Vrije Universiteit, De Boelelaan 1105, 1081 HV Amsterdam, The Netherlands*

(Received 31 March 2023; revised 30 June 2023; accepted 26 October 2023; published 11 December 2023)

Photoinduced phase transitions in correlated materials promise diverse applications from ultrafast switches to optoelectronics. Resolving those transitions and possible metastable phases temporally are key enablers for these applications, but challenge existing experimental approaches. Extreme nonlinear optics can help probe phase changes, as higher-order nonlinearities have higher sensitivity and temporal resolution to band structure and lattice deformations. Here the ultrafast transition from the semiconducting to the metallic phases in polycrystalline thin-film NbO_2 is investigated by time-resolved harmonic spectroscopy. The emission strength of all harmonic orders shows a steplike suppression when the excitation fluence exceeds a threshold ($\sim$11–12 mJ/cm^2), below the fluence required for the thermal transition—a signature of the nonthermal emergence of a metallic phase within 100 ± 20 fs. This observation is backed by full *ab initio* simulations as well as a 1D chain model of high-harmonic generation from both phases. Our results demonstrate femtosecond harmonic probing of phase transitions and nonthermal dynamics in solids.

DOI: 10.1103/PhysRevLett.131.243201

Optical control of exotic or hidden phases in strongly correlated systems has emerged as one of the core topics in condensed matter physics [1,2]. Besides a fundamental interest in disentangling competing electron-electron and electron-lattice interactions, there is an equally attractive technological relevance for the realization of Mott memristors [3–5]. Particularly, photoinduced insulator-to-metal transition (IMT) in strongly correlated materials has been studied widely for decades [3,4,6–9]. Various ultrafast spectroscopy tools such as linear reflection or absorption [7], photoelectron emission [8], and x-ray or electron diffraction [9] were applied to reveal lattice distortions and band structure transformations, and even indications for metastable or hidden states were discovered in photoinduced IMT [8,9]. The substantial achievements made in this area are mostly based on linear or low-order nonlinear spectroscopy, which probes a perturbative response of the bound electronic states.

High-harmonic generation (HHG) is an extreme nonlinear optical effect and has been widely studied in gases for decades and in more recent times also in solids [10,11]. HHG in solids originates from two main contributions: a laser-driven intraband current and an interband polarization, which includes electron-hole recollisions [11,12]. While generalizations are difficult and still under debate, it is mostly accepted that the former effect (intraband) is dominant for below-band-gap harmonics, whereas the latter (interband) mainly contributes to above-band-gap harmonics [11]. Either way, the laser-driven sampling of the band structure in solid HHG implies a high sensitivity of HHG to subtle microscopic changes in electronic and lattice structures [13–20]. Thus high-harmonic spectroscopy has been used for all-optical detections of nanostructures [21], band structure [15,16], dynamical Bloch oscillations [22], and the superconducting phase [17]. Moreover, the exquisite time resolution of high-harmonic

spectroscopy has been utilized to control electron motion in dielectrics with attosecond accuracy [12,23]. These characteristics highlight the remarkable capability of high-harmonic spectroscopy that we apply here to decipher photoinduced IMT processes with high sensitivity and temporal resolution.

The availability and close-room-temperature IMT have made VO_2 ($T_c \sim 340$ K) one of the best-studied strongly correlated materials. However, the low T_c makes thermal IMTs and effects from laser excitation difficult to separate from the nonthermal transition [6,24], which challenges all subsequent efforts to disentangle electron-electron and electron-lattice mechanisms. Therefore, we chose niobium dioxide (NbO_2), a $4d^1$ isovalent compound of VO_2 to implement time-resolved HHG probing of phase transitions. NbO_2 exhibits an IMT between a body-centered tetragonal (bct) semiconducting phase and a regular rutile metallic one, but at a much higher temperature of $T_c \sim 1080$ K [25,26]. In this Letter, the photo-induced nonthermal IMT in the thin film NbO_2 is investigated by time-resolved high-harmonic spectroscopy and identified via a characteristic steplike reduction of HHG efficiency when the excitation surpasses a threshold ($\sim$11–12 mJ/cm^2). The model analysis and theoretical simulations both confirm the remarkable influence of IMT on HHG efficiency reduction. The fluence dependence and the transient change of this steplike reduction also indicate the local growth and the ultrafast timescale features of transient metallization in NbO_2. These results highlight the capability of high-harmonic spectroscopy, and also provide new tools to investigate photoinduced IMTs.

Polycrystalline NbO_2 (115 nm thick) was grown on a c-plane sapphire substrate by reactive bias target ion beam deposition [27–29]. HHG is produced by a 50-fs and 1.8-μm driving pulse [details in [29] in reflection mode and collected by a fiber spectrometer (Fig. 1(a)]. In the time-resolved measurements, pump pulses at 400 nm are used for photocarrier excitation. The pump fluences are varied between 1 to 25 mJ/cm^2 via polarizers and kept below the threshold of permanent degradation. Considering the linear absorption of NbO_2 at 400 nm, the injected carrier density at these fluences is between 1 and 25×10^{20} cm^{-3}.

Figure 1(a) shows an HHG spectrum of NbO_2, where the third, fifth and seventh harmonic orders (HOs) of 1.8 μm can be clearly observed. Because of the polycrystalline nature of NbO_2, no even harmonic orders are observed. The measured HHG wavelengths are well above the direct (1.3 eV) and indirect band gap of the thin film NbO_2 (0.7 eV). Separating the interband and intraband contributions in our simulations [29] suggests that interband contributions are dominant. However, we cannot make a definitive assignment of the mechanism due to the complex band structure complexity of NbO_2, which is also not the main point of our work. The third and fifth harmonic orders

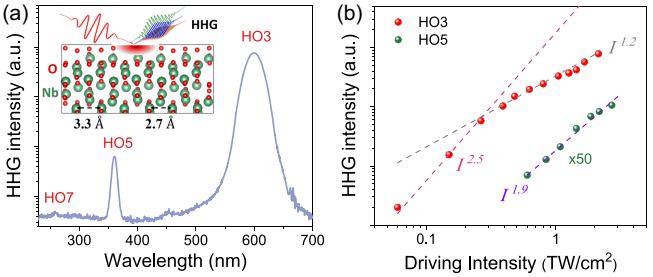

FIG. 1. (a) Static HHG spectrum from NbO_2 thin film, driven by 1.8-μm laser. The third, fifth, and seventh HOs can be clearly observed. The inset displays the experimental reflection configuration. (b) Signals of the third and fifth harmonic orders as a function of the driving intensity. The dashed lines represent fitted power laws.

(HO3 and HO5) as a function of the driving intensity are plotted in Fig. 1(b). The vacuum driving intensity of the 1.8-μm pulse is tuned from 0.05 to 3 TW/cm^2, corresponding to an electric field inside the sample of 0.33 to 2.7 V/nm. For lower intensities, HO3 follows $I^{2.5}$, close to the predicted power law of the perturbative theory. A slope change for HO3 is found when increasing the intensity beyond 0.25 TW/cm^2, where signals are nearly proportional to the driving intensity. Regarding HO5, the measured signal does not follow a power law expected from perturbative behavior but scales with $I^{1.9}$. While HO3 and HO5 are technically not high orders of the nonlinear response, their nonperturbative scaling with laser intensity justifies the classification of the underlying process as HHG. For our work, a high driving intensity (precisely 0.6 TW/cm^2 for HO3 and 1 TW/cm^2 for HO5) guarantees that all harmonic orders result from a nonperturbative nonlinear response.

To investigate HHG in different phases of NbO_2, various pump fluences are applied to excite photocarriers and trigger a potential IMT. Figure 2(a) shows transient spectra of HHG at three pump-probe delays for an excitation fluence of 6 mJ/cm^2 (extended data in Fig. S1 [29]). The photocarrier injection leads to a rapid reduction of all observed harmonic orders, similar to observations in conventional semiconductors [42,43]. It should be noted that the nearly full suppression of HHG signals can persist for hundreds of picoseconds as shown in Fig. S2 [29]. Signal recovery occurs on much longer time scales (not discussed in the present study) and may be affected by the nanosecond photocarrier recombination in NbO_2 [28,44]. Transient changes as a function of pump-probe delay for the integrated harmonics orders HO3 and HO5 are plotted for various excitation fluences in Fig. 2(b) and S3 in [29]. Their dynamic behaviors are similar, but HO5 is suppressed more than HO3 following photocarrier injection, as shown in Fig. S4 [29]. Transient HHG signals reach the maximum suppression within 150 fs. Complete suppression of the signal (corresponding to $\Delta I_{\mathrm{HHG}} = -1$) with increasing

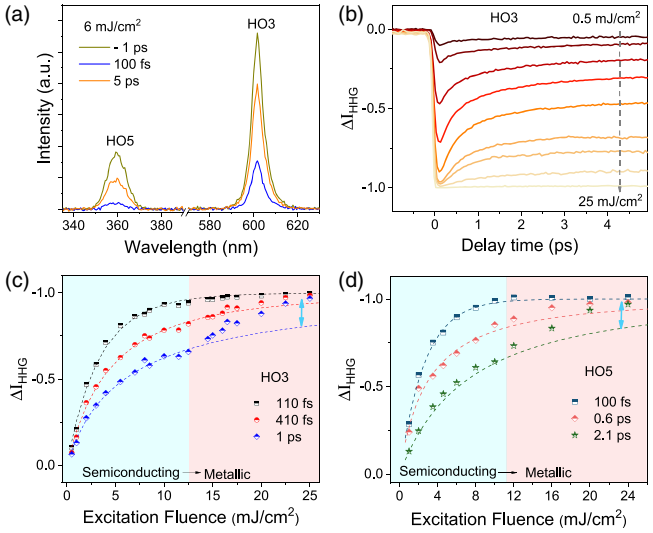

FIG. 2. Time-resolved HHG in NbO_2 thin film. (a) Transient HHG spectra for selected pump-probe delays at excitation fluence of 6 mJ/cm^2. (b) Transient change of HO3 under a series of excitation intensities, where 0 and -1 represent the intact value and full suppression of HHG. (c)–(d) Transient changes of HO3 and HO5 as a function of excitation fluence at several delay times. The dashed lines are fits based on the saturation model.

excitation fluence is possible, enabling to tune nonlinear signals via optical or electronic excitation of carrier density. Subsequently, the HHG signals rapidly recover with a fitted lifetime of 0.3–0.4 ps, especially for low-fluence excitations, possibly related to fast Auger-Meitner recombination. However, this rapid recovery starts to diminish when the excitation becomes stronger, in contrast to the many-body effect in conventional semiconductors. Moreover, full quenching of HHG at the highest fluence can persist for tens of picoseconds without any relaxation, which is only observed in strongly correlated materials [29,45] This gives a first indication of the potential contribution of other mechanisms, such as an IMT, besides classical photocarrier dynamics. Before substantiating that argument, we first examine the dynamic behavior of transient HHG in the semiconducting NbO_2 (at low fluence).

For HHG in solids, photoexcited free carriers have been found to reduce generation efficiency, and both ground-state bleaching by photoexcitation as well as a reduction of the dephasing time have been invoked as possible reasons [42,43,46–48]. To link the HHG suppression to photocarrier density, transient changes of HO3 and HO5 are shown as a function of the excitation fluences in Figs. 2(c)–2(d) for three pump-probe delays. For delays right after time zero (e.g., 110 fs), we observe a signal suppression in HO3 and HO5 with a rapidly increasing slope for low fluences which saturates and shows complete suppression at high fluences. Similar behaviors are observed in the lower driving intensity (perturbative regime) (Fig. S5 [29]), and at longer driving wavelengths (Fig. S6 [29]). We fit the HHG signal suppression right after time zero [110 fs in Figs. 2(c)–2(d)] or at low fluence with a phenomenological saturation model based on the semiconducting response, as detailed in [29]. Importantly, we note that the observed suppression saturation (fit for HO3 and HO5) should be a general feature of photoexcited HHG in semiconductors and dielectrics, and has already been observed for many other materials [42,43,46,47].

For later time delays (> 200 fs) in Figs. 2(c)–2(d), the suppression of HO3 and HO5 at high fluence shows a remarkably different behavior rather than the usual saturation features observed at early delays and previously in the literature. The lower-fluence data again fit well by the saturation model, indicating a typical semiconductor-like response to HHG and its photocarrier-induced suppression. However, for fluences above a threshold F_{th} of 11–12 mJ/cm^2, the HHG suppression shows a stepwise increase (marked by cyan arrows in Fig. 2), which is also observed at the same fluence in independent measurements for HO5 [Fig. 2(d)] and HO3 at a longer driving wavelength (Fig. S6 [29]). This steplike suppression increase and significant deviation from the characteristics of the saturation model is a hallmark sign of an insulator-to-metal phase transition: Once the fluence reaches a threshold for sufficient photocarrier excitation, the supplied carriers modify the potential surface and weaken bonding to trigger metallization, and the emerging metallic phase causes a sudden steplike change in HHG signal. Previous studies on NbO_2 indicated a photoinduced metallization near the same fluence F_{th} by THz and coherent phonon spectroscopic [28,49]. HHG spectra have been reported in several strongly correlated materials theoretically [14,45,50–52] and experimentally, including time-resolved measurements of VO_2 [45], but such steplike suppression has not been reported before and considered as robust evidence for phase transition.

To reinforce the above interpretation of photoinduced IMT revealed by HHG, simulations of the HHG process have been performed for both the semiconducting and metallic phases of NbO_2, by means of a combined approach of *ab initio* methods and solving the semiconductor Bloch equations [29,40]. As shown in Fig. 3(a), the band structures of these two phases (metallic rutile, and semiconducting *bct*) are calculated by density functional theory (DFT) and projected onto Wannier orbitals to solve electron dynamics numerically. Figure 3(b) shows the calculated HHG spectra from the two distinct phases of NbO_2, based on the experimental parameters used above. Stronger HHG signals can be observed in the bct phase than in the rutile one, consistent with experimental observation, where the metallic phase has a lower nonlinear efficiency. As shown in the inset of Fig. 3(b), HO3 in the rutile phase is less than half of that in the bct phase. Such efficiency difference is enhanced in HO5, supporting the conclusion from Fig. 2, that higher-order nonlinearities are more sensitive to

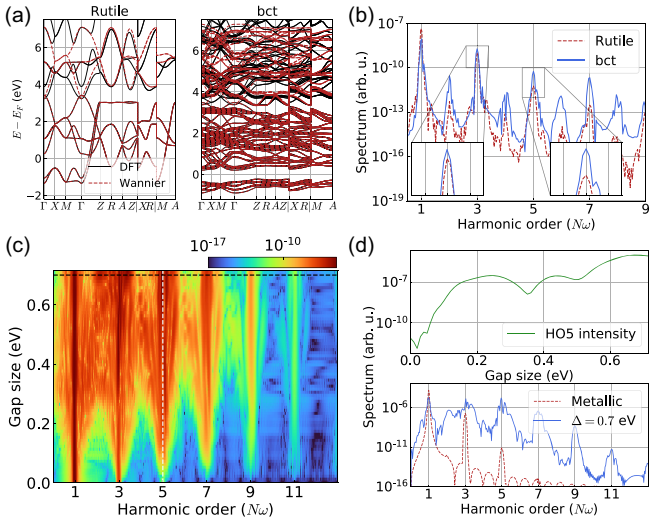

FIG. 3. Theoretical simulations of HHG spectra in NbO_2. (a) DFT band structure for both the metallic rutile and semiconducting *bct* phases. Black lines depict the full DFT calculation while red ones show the band structure after a Wannierization procedure. (b) HHG spectra in the rutile and bct phase, using the full *ab initio* model for the NbO_2. The insets depict a zoom around HO3 and HO5, respectively. (c) HHG spectra of the Peierls model in terms of the gap size. (d) Two snapshots of (c). The upper panel, corresponding to the vertical white line in (c), depicts the intensity of the fifth harmonic as a function of the gap size. The lower panel, extracted from the horizontal black line in (c), shows the HHG spectra comparison between the metallic and insulating phases (with a gap of 0.7 eV which is roughly the gap in NbO_2).

metallization. Interestingly one can also find a larger fundamental harmonic signal (i.e., $N = 1$) in the rutile, compared with the bct, which could be attributed to the high reflection efficiency of the metallic phase and interpreted as evidence of the IMT. The transient reflection change of our sample in Fig. S8 [29] reproduced this phenomenon and also verifies the validity of our simulations. Thus, HHG simulations in NbO_2 under different phases demonstrate that metallic formation can indeed abruptly and significantly reduce HHG efficiency. To highlight the remarkable influence of metallization on HHG efficiency, we further performed another numerical simulation using a modified version of the Peierls model (see [29] for more details). The effect of the band gap on the HHG spectra is explored and the corresponding results are shown in Figs. 3(c)–3(d). The HHG spectrum and efficiency are extremely sensitive to band gap variations. In the upper panel of Fig. 3(d), the gap shrinkage results in a gradual efficiency reduction of HO5. This effect may play a limited role in transient HHG changes, but cannot explain the anomalous steplike deviation from the saturation model in Figs. 2(c)–2(d). The complete collapse of the band gap, leading to a sudden and considerable drop in HHG efficiency in the upper panel of Fig. 3(d), can provide us with a reasonable answer: once the excitation fluence exceeds F_{th}, the system enters a transient metallic phase and thus HHG signals are nearly completely deactivated, as shown in Fig. 3(d). Therefore, metallization (i.e., band gap collapse) beyond F_{th}, accounts for the obvious deviation from the saturation model in Figs. 2(c)–2(d), corroborating our interpretation of the observation of photoinduced phase transition.

Figures 2 and 3 establish the presence and sensitivity of HHG to an IMT. Moreover, we have shown that the saturation model captures transient HHG from the semiconducting phase below F_{th}, and transient metallization leads to a steplike deviation at higher fluence. Thus, to isolate the transient emergence of the metallic phase from the general transient semiconducting response following photoexcitation, we subtract the fitted saturation model from transient data in Fig. 2 for all time delays. The isolated HHG responses are interpreted as the emergence of the metallic phase and the corresponding phase fraction can be calculated and plotted in Fig. 4(a) as a function of the excitation fluence for various time delays (details in [29]). After time zero, the metallic phase fraction starts increasing with the excitation fluence ($> F_{\mathrm{th}}$) but stays similar for a long delay time. The fluence-dependent phase fraction is indicative of a spatially inhomogeneous transition, and such an explanation is also supported by the observation that the significant deviation in Figs. 2(c)–2(d) above F_{th} is rather gradual than abrupt. In fact, similar nanoscale nucleation has also been found in other phase-transition materials via modern nano-imaging techniques and assigned to crystal imperfections [6,53]. Besides spatial information on the IMT, the isolated IMT response in the time domain also allows tracking its emergence timescale. The inset of Fig. 4(b) displays the transient responses of the metallic phase for selected fluences, which shows that the IMT responses are absent for low fluence and only exist when the excitation fluence exceeds the threshold F_{th}—key signatures of phase transitions. Following photoexcitation at high fluence, the transient response from IMT emerges rapidly and the HHG suppression lasts long. Its emergence rate corresponds to the timescale of the IMT, and the extracted full width at half maximum (FWHM) of these rates are plotted in Fig. 4(b) and the fitting process can be found in [29]. The timescale of IMT seems constant (from 110 to 90 fs) within error bars (20 fs), below the instrumental resolution (~70 fs) in our experiment. The direct fitting of transient HO3 changes in Fig. S10 [29] also leads to the same conclusion: the rising edge becomes sharper when transient metallization occurs and eventually shows the shortest FWHM of 105 fs.

Such a short timescale of IMT benefits discovering the driving forces of the IMT. According to the thermal capacity of NbO_2 [54], the *upper* limit of the lattice temperature induced by laser heating is estimated to be < 500 K at F_{th}, much lower than the phase transition

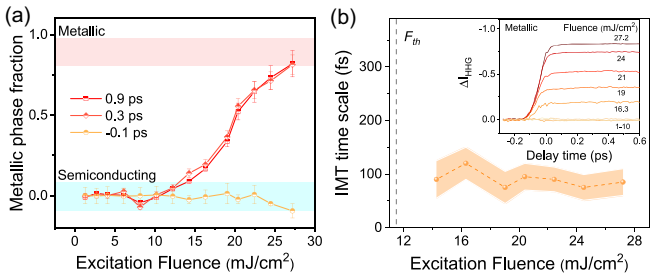

FIG. 4. Phase diagram and time scale of IMT (a) Metallic phase fraction as a function of the excitation fluence, calculated from the difference between transient HHG signals and the saturation model in Fig. 2. (b) Timescale of phase transition, extracted from transient HHG response of newly emerging metallic phase. The inset shows the transient response of the metallic phase at different fluences. The FWHMs of the emergence rate of the metallic phase are fitted and taken as the timescale of phase transition.

temperature ($T_c \sim 1080$ K). (The estimation details seen in [29].) This not only confirms the nonthermal nature of transient metallization in NbO_2, but also means that the lattice transformation has no obvious contribution to the steplike variation of the emitted harmonics, and transient metallization with the bct lattice, as intermediate states, may be an ultrafast and nonthermal phase transition [7–9]. It should be highlighted that transient metallization without complete lattice transformation does not justify an interpretation of a pure breakdown of electron-electron correlation (Mott interaction) following excitation. Ultrafast and local lattice distortion has also been found near F_{th} via coherent phonon spectroscopy [28], and the timescale we measured in the present study is close to a half period of the phonon mode, mainly for dissociating the Nb-Nb dimer—the characteristic lattice change in the temperature-induced IMT. This motivates revisiting the current experiments with even shorter pulses in order to distinguish structurally driven (Nb-Nb dimer dissociation) from electronically driven (Mott) transitions by their different timescales.

Our experiment represents the first unambiguous evidence of photoinduced IMT in strongly correlated materials via transient high-harmonic spectroscopy, which is apparent as a large deviation of transient HHG from the typical semiconductor response following photoexcitation. This method can be regarded as a robust strategy and general evidence for measuring photoinduced IMTs in strongly correlated materials using HHG. Our experimental findings are fully supported by HHG calculations from both the *ab initio* theory in NbO_2 and a Peierls model. Moreover, our analysis supports a local nucleation process and ultrafast metallization process emerging with nanotexture for fluences just above the threshold. The timescale of the phase transition of 100 fs which we extract from our data indicates a nonthermal transition, which motivates experiments with even higher time resolution and ideally spatial resolution to address the emergent nanotexture that was indirectly inferred from our data. Finally, we note that the near-complete signal suppression observed at high fluences in NbO_2 makes it an ideal candidate for all-optical switches and control, a key aspiration for ultrafast IMTs and strongly correlated materials.

Part of this work has been carried out at the Advanced Research Center for Nanolithography (ARCNL), a public-private partnership of the University of Amsterdam (UvA), the Vrije Universiteit Amsterdam (VU), the Netherlands Organisation for Scientific Research (NWO), and the semiconductor equipment manufacturer ASML, and was partly financed by "Toeslag voor Topconsortia voor Kennis en Innovatie (TKI)" from the Dutch Ministry of Economic Affairs and Climate Policy. This manuscript is part of a project that has received funding from the European Research Council (ERC) under the European Union's Horizon Europe research and innovation programme (Grant Agreement No. 101041819, ERC Starting Grant ANACONDA). Z. N., L. G., and P. M. K. acknowledge support from the Open Technology Programme (OTP) by NWO, Grant No. 18703. P. J. acknowledges funding by the German Research Foundation—SFB1477 "Light-Matter Interaction at Interfaces," Project No. 441234705. E. B. M. and R. E. F. S. acknowledge support from the fellowship LCF/BQ/PR21/11840008 from "La Caixa" Foundation (ID 100010434). This research was supported by Grant No. PID2021-122769NB-I00 funded by MCIN/AEI. R. E. F. S. also acknowledges fruitful discussions with Eduardo R. Hernández.

*z.nie@arcnl.nl
†p.kraus@arcnl.nl

[1] M. Rini, R. Tobey, N. Dean, J. Itatani, Y. Tomioka, Y. Tokura, R. W. Schoenlein, and A. Cavalleri, Control of the electronic phase of a manganite by mode-selective vibrational excitation, Nature (London) **449**, 72 (2007).
[2] J. G. Horstmann, H. Böckmann, B. Wit, F. Kurtz, G. Storeck, and C. Ropers, Coherent control of a surface structural phase transition, Nature (London) **583**, 232 (2020).
[3] M. Imada, A. Fujimori, and Y. Tokura, Metal-insulator transitions, Rev. Mod. Phys. **70**, 1039 (1998).
[4] Z. Yang, C. Ko, and S. Ramanathan, Oxide electronics utilizing ultrafast metal-insulator transitions, Annu. Rev. Mater. Res. **41**, 337 (2011).
[5] S. Kumar, R. S. Williams, and Z. Wang, Third-order nanocircuit elements for neuromorphic engineering, Nature (London) **585**, 518 (2020).
[6] D. Wegkampand J. Stähler, Ultrafast dynamics during the photoinduced phase transition in VO_2, Prog. Surf. Sci. **90**, 464 (2015).
[7] M. F. Jager, C. Ott, P. M. Kraus, C. J. Kaplan, W. Pouse, R. E. Marvel, R. F. Haglund, D. M. Neumark, and S. R. Leone, Tracking the insulator-to-metal phase transition in

VO_2 with few-femtosecond extreme uv transient absorption spectroscopy, Proc. Natl. Acad. Sci. U.S.A. **114**, 9558 (2017).

[8] D. Wegkamp, M. Herzog, L. Xian, M. Gatti, P. Cudazzo, C. L. McGahan, R. E. Marvel, R. F. Haglund Jr, A. Rubio, M. Wolf *et al.*, Instantaneous band gap collapse in photoexcited monoclinic VO_2 due to photocarrier doping, Phys. Rev. Lett. **113**, 216401 (2014).

[9] V. R. Morrison, R. P. Chatelain, K. L. Tiwari, A. Hendaoui, A. Bruhács, M. Chaker, and B. J. Siwick, A photoinduced metal-like phase of monoclinic VO_2 revealed by ultrafast electron diffraction, Science **346**, 445 (2014).

[10] S. Ghimire, A. D. DiChiara, E. Sistrunk, P. Agostini, L. F. DiMauro, and D. A. Reis, Observation of high-order harmonic generation in a bulk crystal, Nat. Phys. **7**, 138 (2011).

[11] S. Ghimire and D. A. Reis, High-harmonic generation from solids, Nat. Phys. **15**, 10 (2019).

[12] G. Vampa, T. Hammond, N. Thiré, B. Schmidt, F. Légaré, C. McDonald, T. Brabec, and P. Corkum, Linking high harmonics from gases and solids, Nature (London) **522**, 462 (2015).

[13] T. T. Luu and H. J. Wörner, Measurement of the berry curvature of solids using high-harmonic spectroscopy, Nat. Commun. **9**, 916 (2018).

[14] R. Silva, I. V. Blinov, A. N. Rubtsov, O. Smirnova, and M. Ivanov, High-harmonic spectroscopy of ultrafast many-body dynamics in strongly correlated systems, Nat. Photonics **12**, 266 (2018).

[15] M. Borsch, C. P. Schmid, L. Weigl, S. Schlauderer, N. Hofmann, C. Lange, J. Steiner, S. Koch, R. Huber, and M. Kira, Super-resolution lightwave tomography of electronic bands in quantum materials, Science **370**, 1204 (2020).

[16] J. Costello, S. O'Hara, Q. Wu, D. Valovcin, L. Pfeiffer, K. West, and M. Sherwin, Reconstruction of Bloch wave functions of holes in a semiconductor, Nature (London) **599**, 57 (2021).

[17] J. Alcalà, U. Bhattacharya, J. Biegert, M. Ciappina, U. Elu, T. Graß, P. T. Grochowski, M. Lewenstein, A. Palau, T. P. Sidiropoulos *et al.*, High-harmonic spectroscopy of quantum phase transitions in a high-T_c superconductor, Proc. Natl. Acad. Sci. U.S.A. **119**, e2207766119 (2022).

[18] C. P. Schmid, L. Weigl, P. Grössing, V. Junk, C. Gorini, S. Schlauderer, S. Ito, M. Meierhofer, N. Hofmann, D. Afanasiev *et al.*, Tunable non-integer high-harmonic generation in a topological insulator, Nature (London) **593**, 385 (2021).

[19] E. B. Molinero and R. E. F. Silva, Coherent control of the photoinduced transition in a strongly correlated material, Phys. Rev. Res. **4**, 043198 (2022).

[20] A. J. Uzan-Narovlansky, Á. Jiménez-Galán, G. Orenstein, R. E. Silva, T. Arusi-Parpar, S. Shames, B. D. Bruner, B. Yan, O. Smirnova, M. Ivanov *et al.*, Observation of light-driven band structure via multiband high-harmonic spectroscopy, Nat. Photonics **16**, 428 (2022).

[21] S. D. C. Roscam Abbing, R. Kolkowski, Z.-Y. Zhang, F. Campi, L. Lötgering, A. F. Koenderink, and P. M. Kraus, Extreme-ultraviolet shaping and imaging by high-harmonic generation from nanostructured silica, Phys. Rev. Lett. **128**, 223902 (2022).

[22] O. Schubert, M. Hohenleutner, F. Langer, B. Urbanek, C. Lange, U. Huttner, D. Golde, T. Meier, M. Kira, S. W. Koch *et al.*, Sub-cycle control of terahertz high-harmonic generation by dynamical Bloch oscillations, Nat. Photonics **8**, 119 (2014).

[23] J. Freudenstein, M. Borsch, M. Meierhofer, D. Afanasiev, C. P. Schmid, F. Sandner, M. Liebich, A. Girnghuber, M. Knorr, M. Kira *et al.*, Attosecond clocking of correlations between bloch electrons, Nature (London) **610**, 290 (2022).

[24] L. Vidas, D. Schick, E. Martínez, D. Perez-Salinas, A. Ramos-Álvarez, S. Cichy, S. Batlle-Porro, A. S. Johnson, K. A. Hallman, R. F. Haglund Jr *et al.*, Does VO_2 host a transient monoclinic metallic phase?, Phys. Rev. X **10**, 031047 (2020).

[25] G. Belanger, J. Destry, G. Perluzzo, and P. Raccah, Electron transport in single crystals of niobium dioxide, Can. J. Phys. **52**, 2272 (1974).

[26] A. O'Hara and A. A. Demkov, Nature of the metal-insulator transition in NbO_2, Phys. Rev. B **91**, 094305 (2015).

[27] Y. Wang, R. B. Comes, S. Kittiwatanakul, S. A. Wolf, and J. Lu, Epitaxial niobium dioxide thin films by reactive-biased target ion beam deposition, J. Vac. Sci. Technol. A **33**, 021516 (2015).

[28] Y. Wang, Z. Nie, Y. Shi, Y. Wang, and F. Wang, Coherent vibrational dynamics of NbO_2 film, Phys. Rev. Mater. **6**, 035005 (2022).

[29] See Supplemental Material at http://link.aps.org/supplemental/10.1103/PhysRevLett.131.243201 for details of experimental measurement, the saturation model, and theoretical models. It includes Refs. [30–41].

[30] K. Shibuya and A. Sawa, Epitaxial growth and polarized raman scattering of niobium dioxide films, AIP Adv. **12**, 055103 (2022).

[31] G. J. Páez Fajardo, S. A. Howard, E. Evlyukhin, M. J. Wahila, W. R. Mondal, M. Zuba, J. E. Boschker, H. Paik, D. G. Schlom, J. T. Sadowski *et al.*, Structural phase transitions of NbO_2: Bulk versus surface, Chem. Mater. **33**, 1416 (2021).

[32] G. de Haan, T. van Den Hooven, and P. Planken, Ultrafast laser-induced strain waves in thin ruthenium layers, Opt. Express **29**, 32051 (2021).

[33] H. Nishidome, K. Nagai, K. Uchida, Y. Ichinose, Y. Yomogida, Y. Miyata, K. Tanaka, and K. Yanagi, Control of high-harmonic generation by tuning the electronic structure and carrier injection, Nano Lett. **20**, 6215 (2020).

[34] G. G. Brown, Á. Jiménez-Galán, R. E. Silva, and M. Ivanov, A real-space perspective on dephasing in solid-state high harmonic generation, arXiv:2210.16889.

[35] P. C. Becker, H. L. Fragnito, C. B. Cruz, R. Fork, J. Cunningham, J. Henry, and C. Shank, Femtosecond photon echoes from band-to-band transitions in GaAs, Phys. Rev. Lett. **61**, 1647 (1988).

[36] Y. Sakai, N. Tsuda, and T. Sakata, Electrical properties of semiconducting NbO_2, J. Phys. Soc. Jpn. **54**, 1514 (1985).

[37] Y. Cheng, H. Hong, H. Zhao, C. Wu, Y. Pan, C. Liu, Y. Zuo, Z. Zhang, J. Xie, J. Wang *et al.*, Ultrafast optical modulation of harmonic generation in two-dimensional materials, Nano Lett. **20**, 8053 (2020).

[38] P. Giannozzi *et al.*, Quantum espresso: A modular and open-source software project for quantum simulations of materials, J. Phys. Condens. Matter **21**, 395502 (2009).

[39] A. A. Mostofi, J. R. Yates, G. Pizzi, Y.-S. Lee, I. Souza, D. Vanderbilt, and N. Marzari, An updated version of WANNIER90: A tool for obtaining maximally-localised Wannier functions, Comput. Phys. Commun. **185**, 2309 (2014).

[40] R. E. F. Silva, F. Martín, and M. Ivanov, High harmonic generation in crystals using maximally localized Wannier functions, Phys. Rev. B **100**, 195201 (2019).

[41] D. Vanderbilt, *Berry Phases in Electronic Structure Theory* (Cambridge University Press, Cambridge, England, 2018).

[42] Z. Wang, H. Park, Y. H. Lai, J. Xu, C. I. Blaga, F. Yang, P. Agostini, and L. F. DiMauro, The roles of photo-carrier doping and driving wavelength in high harmonic generation from a semiconductor, Nat. Commun. **8**, 1686 (2017).

[43] C. Heide, Y. Kobayashi, A. C. Johnson, F. Liu, T. F. Heinz, D. A. Reis, and S. Ghimire, Probing electron-hole coherence in strongly driven 2d materials using high-harmonic generation, Optica **9**, 512 (2022).

[44] J. K. Clark, Y.-L. Ho, H. Matsui, H. Tabata, and J.-J. Delaunay, Thresholdless behavior and linearity of the optically induced metallization of NbO_2, Phys. Rev. Res. **1**, 033168 (2019).

[45] M. R. Bionta, E. Haddad, A. Leblanc, V. Gruson, P. Lassonde, H. Ibrahim, J. Chaillou, N. Émond, M. R. Otto, Á. Jiménez-Galán *et al.*, Tracking ultrafast solid-state dynamics using high harmonic spectroscopy, Phys. Rev. Res. **3**, 023250 (2021).

[46] Y. Wang, F. Iyikanat, X. Bai, X. Hu, S. Das, Y. Dai, Y. Zhang, L. Du, S. Li, H. Lipsanen *et al.*, Optical control of high-harmonic generation at the atomic thickness, Nano Lett. **22**, 8455 (2022).

[47] K. Nagai, K. Uchida, S. Kusaba, T. Endo, Y. Miyata, and K. Tanaka, Effect of incoherent electron-hole pairs on high harmonic generation in atomically thin semiconductors, arXiv:2112.12951.

[48] K. S. Shimomura *et al.*, Ultrafast electron-electron scattering in metallic phase of 2H-$NbSe_2$ probed by high harmonic generation, arXiv:2302.04984.

[49] R. Rana, J. M. Klopf, J. Grenzer, H. Schneider, M. Helm, and A. Pashkin, Nonthermal nature of photoinduced insulator-to-metal transition in NbO_2, Phys. Rev. B **99**, 041102(R) (2019).

[50] N. Tancogne-Dejean, M. A. Sentef, and A. Rubio, Ultrafast modification of Hubbard U in a strongly correlated material: *ab initio* high-harmonic generation in NiO, Phys. Rev. Lett. **121**, 097402 (2018).

[51] S. Imai, A. Ono, and S. Ishihara, High harmonic generation in a correlated electron system, Phys. Rev. Lett. **124**, 157404 (2020).

[52] K. Uchida, G. Mattoni, S. Yonezawa, F. Nakamura, Y. Maeno, and K. Tanaka, High-order harmonic generation and its unconventional scaling law in the Mott-insulating Ca_2RuO_4, Phys. Rev. Lett. **128**, 127401 (2022).

[53] S. A. Donges, O. Khatib, B. T. O'Callahan, J. M. Atkin, J. H. Park, D. Cobden, and M. B. Raschke, Ultrafast nanoimaging of the photoinduced phase transition dynamics in VO_2, Nano Lett. **16**, 3029 (2016).

[54] K. Jacob, C. Shekhar, M. Vinay, and Y. Waseda, Thermodynamic properties of niobium oxides, J. Chem. Eng. Data **55**, 4854 (2010).